

1-1-2000

Waste Isolation Pilot Plant Shaft Seal Salt Consolidation Modelling

Mary P. Cardenas
Harvey Mudd College

William Statham
Duke Engineering and Services Incorporated

Recommended Citation

Cardenas, M.P. and Statham, W. "Waste Isolation Pilot Plant Shaft Seal Salt Consolidation Modelling," *Computational Methods for Subsurface Flow and Transport*, 1, Proceedings of the XIII International Conference on Computational Methods in Water Resources, pp. 37-44, A.A. Balkema, Rotterdam/Brookfield, 2000.

This Book Chapter is brought to you for free and open access by the HMC Faculty Scholarship at Scholarship @ Claremont. It has been accepted for inclusion in All HMC Faculty Publications and Research by an authorized administrator of Scholarship @ Claremont. For more information, please contact scholarship@cuc.claremont.edu.

Waste isolation pilot plant shaft seal salt consolidation modelling

M.P. Cardenas

Harvey Mudd College, Claremont, Calif., USA

W. Statham

Duke Engineering and Services Incorporated, Austin, Tex., USA

ABSTRACT: The numerical code *TOUGH28W* was modified to calculate porosity and permeability changes due to salt consolidation. The porosity change was modeled as a function of pore pressure and depth in the salt. The permeability was coupled to the porosity using log-linear models. The Waste Isolation Pilot Plant (*WIPP*) lower shaft seals and surrounding formation were modeled. Crushed salt is one of the key components of the sealing system, and to gain understanding of the consolidation of the crushed salt after seal emplacement, *TOUGH28W* simulations were performed. The results showed the salt consolidation is greatly affected by the pore pressure. After 100 years of simulation, the porosity of the crushed salt for a log-linear model has decreased from 0.1 to a value of 0.035 at the bottom of the crushed salt column and the minimum permeability in the crushed salt column after 100 years of consolidation is $4 \times 10^{-22} \text{ m}^2$.

1 INTRODUCTION

The Waste Isolation Pilot Plant (*WIPP*) is a repository funded by the United States Department of Energy (*DOE*) and governed by federal regulation. *WIPP* is located 51.5 km east of Carlsbad, New Mexico, and is used for transuranic waste disposal in halite. The repository consists of a network of drifts, panels, and disposal rooms excavated from bedded salt within the Salado formation. The Salado formation is 655 m below the surface, and consists of beds of relatively pure and impure halite with interspersed clay and polyhalite. Four vertical shafts provide service access to the underground repository. After waste disposal operations at *WIPP* are completed, these four shafts will be permanently sealed. This is to prevent release of contaminants to the biosphere. Seal materials consist of crushed salt, bentonite clay, and salt-saturated concrete. The shaft sealing system is shown conceptually in Figure 1 in relation to the principle stratigraphic units at the site. A key component of the design is the compacted salt column, approximately 172-m thick, in the lower portion of the shafts. This component is composed of crushed salt taken from the host Salado formation, which will be compacted during construction to a fractional density of 0.9 (a density of approximately 90% of the intact Salado salt density). After the seal is emplaced, further compaction of the crushed salt will occur as the host salt formation creeps inward on

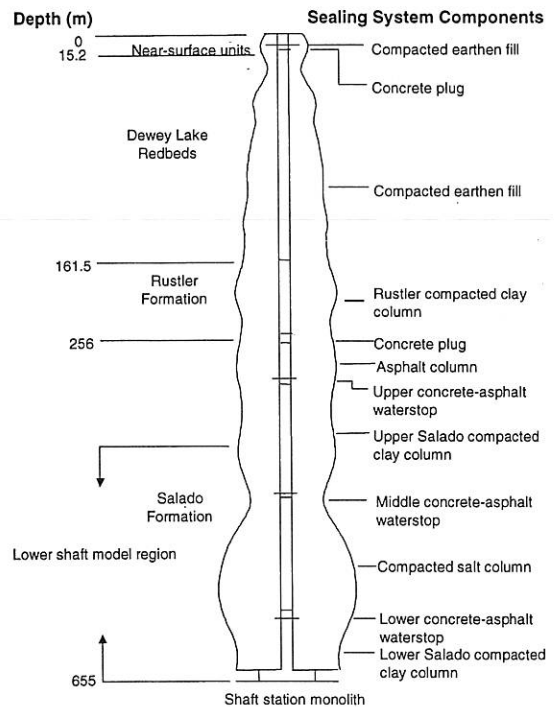


Figure 1. Schematic of shaft sealing system and stratigraphic units.

the shaft excavation. Laboratory tests have shown that the crushed salt will consolidate and achieve permeability comparable to that of undisturbed halite

(Brodsky 1994.) Also, tests have shown that porosity decreases as the halite heals in response to applied load (Holcomb & Zeuch 1990, Zeuch 1990). A structural analysis was undertaken (Sandia 1996) that indicated the development of increasing fluid pressure within the crushed salt could reduce the closure rate of the shaft, and therefore, the consolidation of the crushed salt. To investigate the effect of fluid pressure on the consolidation of the crushed salt in the lower shaft seals, a fluid flow analysis was performed.

TOUGH28W (Christian-Frear 1996) is a version of *TOUGH2* (Pruess 1987, 1991). It is essentially *TOUGH2* with an equation of state module for brine and hydrogen. *TOUGH28W* was modified in order to simulate crushed salt consolidation in the lower shaft model. Previously, Statham modeled crushed salt consolidation as an absolute permeability change as a function of pore pressure and depth (Statham et al. 1997). For these simulations, Statham kept the crushed salt porosity constant. Porosity changes were not considered because *TOUGH28W* could not handle a porosity change without adversely affecting the mass balance (i.e., mass could not be conserved if porosity changed.) We modified *TOUGH28W* so that a porosity change would not cause mass balance problems.

To model the crushed salt porosity changes, we used results from Callahan's crushed-salt constitutive model of the shaft seal consolidation (Callahan 1999a). We developed an equation fitting this data which describes the time rate of change of porosity as a function of pore pressure and depth. This equation was implemented into *TOUGH28W*, and lower shaft model simulations were performed to determine the effect of the crushed-salt consolidation on the performance. Specifically, values of porosity and permeability in the crushed salt column as a function of time were of interest, since these give an indication of the seal performance.

2 THEORY

Previously, Statham modeled crushed-salt consolidation in *TOUGH28W* as an absolute permeability change (with constant porosity). Porosity changes due to crushed salt consolidation have not previously been modeled with *TOUGH28W*. This is because porosity changes were not allowable in *TOUGH28W* due to mass balance considerations. The *TOUGH28W* model equations are based on conservation of mass, written as:

$$\frac{d}{dt} \int_{V_n} M^{(\kappa)} dv = \int_{\Gamma_n} F^{(\kappa)} \cdot n d\Gamma + \int_{V_n} q^{(\kappa)} dv \quad (1)$$

where $\kappa=1$: brine, 2: hydrogen, V_n = an arbitrary flow domain (in our case, an element of the mesh),

and Γ_n = an area over which flux occurs (for example, a face of an element).

$$F^{(\kappa)} = \sum_{\beta=1,g} F_{\beta}^{(\kappa)} \quad \text{are the mass flux per volume terms, a sum over phases} \quad (2)$$

where β = phase (liquid or gas), n = unit direction vector, q = sources or sinks per volume

$$M^{(\kappa)} = \phi \sum_{\beta=1,g} S_{\beta} \rho_{\beta} X_{\beta}^{(\kappa)} \quad \text{are the mass accumulation terms per volume} \quad (3)$$

where ϕ = porosity, S_{β} = saturation of phase β , ρ_{β} = density of phase β , $X_{\beta}^{(\kappa)}$ = mass fraction of component κ in phase β .

The problem is the mass accumulation term, equation 3. As the porosity changes, the mass will change. If porosity decreases, the mass will decrease; if the porosity increases, the mass will increase. Therefore, as *TOUGH28W* was initially written, a change in porosity will create a situation where fluid mass will not be conserved.

To address this situation, we followed the work of Javeri (1998). His idea was to inject or remove an amount of mass at each time step based on a porosity change. The components for the *WIPP* lower shaft seal are brine and hydrogen, and only brine is in the liquid phase.

The mass of brine in the liquid phase is $m_{b,liq}$, defined as:

$$m_{b,liq} = \phi S_{liq} \rho_{liq} X_{liq}^b V \quad (4)$$

where ϕ is porosity, S_{liq} is the liquid saturation, X_{liq}^b is the mass fraction of brine in the liquid phase (which will be equal to one for this application, as only brine is in the liquid phase), and V is the volume of the element. To calculate a time rate of change in the liquid brine mass due to a porosity change, we take the time derivative of Eqn. 4, using the chain rule:

$$\frac{dm_{b,liq}}{dt} = \frac{dm_{b,liq}}{d\phi} \frac{d\phi}{dt} = S_{liq} \rho_{liq} X_{liq}^b V \frac{d\phi}{dt} \quad (5)$$

To address the change in gas mass due to a porosity change, similarly:

$$\frac{dm_{gas}}{dt} = S_{gas} \rho_{gas} V \frac{d\phi}{dt} \quad (6)$$

These time rates of change of mass (equations 5 and 6) are the injection or removal rates needed to counterbalance the mass loss or gain due to the porosity change.

The remaining equations in *TOUGH28W* are described in Christian-Frear (1996) and Pruess (1987, 1991), and details may be found in those documents.

3 DATA

A numerical study was performed by Callahan (1999a,b) to determine the effects of pore pressure and depth on the consolidation of crushed salt in a shaft seal. Callahan's crushed salt constitutive model was calibrated using laboratory and field data. The model results were in the form of fractional density versus time for pore pressures of 0, 1, 2 and 4 MPa, and depths of 430, 515, and 600 m. These depths are representative of the top, the middle, and the bottom of the salt column, respectively. Figure 2 shows fractional density for a depth of 515 m, and pore pressures of 0, 1, 2, and 4 MPa. The crushed salt has an initial fractional density of 90%. A fractional density of 100% indicates the crushed salt has achieved a density equal to that of intact salt (i.e., it has consolidated.) In Figure 2, the case with a zero pore pressure (the solid line) shows the fastest consolidation. It has achieved a fractional density of nearly 100% in 120 years. In contrast, the simulation with a pore pressure of 4 MPa (the dot-dot-dashed line) has only reached a fractional density of 93% in 450 years. The simulations at different depths show a similar trend for pore pressure. Using Callahan's results, we described the time rate of change of fractional density as a function of pore pressure and depth. The functional form is:

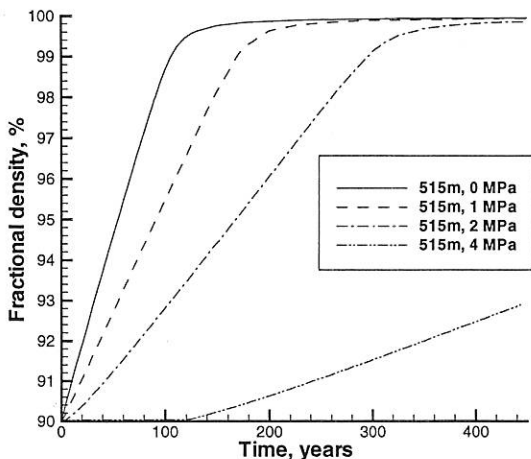


Figure 2. Fractional density versus time as a function of pore pressure and depth.

$$\frac{d\bar{\rho}}{dt} = 2.29 \times 10^{-17} d^5 e^{-0.4P} \quad (7)$$

where $\frac{d\bar{\rho}}{dt}$, time rate of change of fractional density, is in years⁻¹, when d is depth in meters, and P is pore pressure in MPa.

TOUGH28W uses porosity, rather than fractional density, so we related fractional density and porosity as follows:

$$\phi = 0.9(1 - \bar{\rho}) + 0.01 \quad (8)$$

$$\frac{d\phi}{dt} = -0.9 \frac{d\bar{\rho}}{dt} = -2.061 \times 10^{-17} d^5 e^{-0.4P} \quad (9)$$

where $\frac{d\phi}{dt}$ is in years⁻¹ when depth is in meters, and pressure is in MPa.

4 LOWER SHAFT MODEL

All the analyses examined in this document were performed on the lower shaft model. They all use the same geometry and rock properties (except for properties describing the salt column), and boundary conditions described in Statham et al. (1997). The main differences between Statham's analyses and the new analyses described in this paper are the models used to describe the crushed salt consolidation.

The lower shaft geometry was modeled as a two-dimensional radially-symmetric cylindrical grid, and extends in the vertical direction from the base of the shaft (at depth 653-m) up to the top of the Vaca Triste unit (at depth 409 m). The radial extent is from the center of the shaft to the outer radial boundary at 282 m. Figure 3 shows the mesh, with the radial direction truncated at 30 m to show detail. The innermost 4 columns of grid cells represent the shaft and associated seal materials. The next two columns radially outward represent a disturbed rock zone (*DRZ*) surrounding the shaft. Radially outward from the *DRZ* is the Salado Formation stratigraphy, conceptualized as layers of halite separated by several layers of anhydrite and polyhalite marker beds. The marker beds are the shaded areas in Figure 3.

The model components include the components of the seal, and the formation, which consists of halite and marker beds. More specifically, the seal components include asphalt columns, concrete plugs, asphalt waterstops, compacted clay, compacted salt, and the shaft station monolith. The disturbed and undisturbed permeability and porosity of

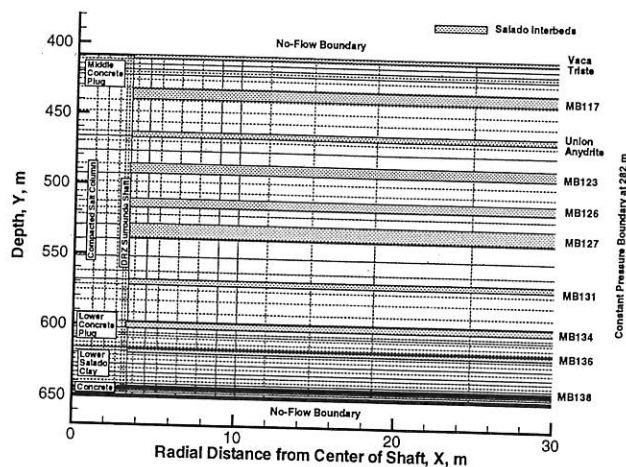


Figure 3. Numerical grid for the lower shaft and surrounding formation.

the host formation units may be found in Statham et al. (1997).

Statham modeled the development of a disturbed rock zone adjacent to the shaft as an increased permeability in the *DRZ*. The disturbed zone develops during the period when the shaft is open. The salt becomes disturbed due to stress fracturing of the host formation around the shaft excavation. After seal emplacement, the *DRZ* will begin to heal around rigid shaft components as the host salt creeps inward. With time, the *DRZ* permeability will heal to the undisturbed values. The healing schedule for the *DRZ* in the lower shaft model is presented in Statham et al. (1997).

Two different sources of fluid movement towards the salt column were considered in the base case: 1.) Gas flow up through the shaft sealing components and *DRZ* from the repository. Gas generation could occur due to corrosive and biochemical reactions within the waste in the repository. 2.) Brine flow toward the shaft from the host Salado Formation due to pressure gradients established during the period the shaft is open to atmosphere. Initially, a large pressure gradient will exist between the host formation (which will be at undisturbed values at some radial distance from the shaft) and the shaft (which had been open to atmospheric pressure.)

Because of the presence of both brine and gas, a multiphase fluid model is required for this analysis. The two-phase flow properties are specified in terms of capillary pressure and relative permeability characteristic curves. These functions may be estimated, for example, using the relationships of Brooks and Corey (1996), van Genuchten (1980), Parker et al. (1987) and others. The van Genuchten-Parker model (Webb 1996, Parker et al. 1987) for capillary pressure and relative permeability was used for all materials in the salt column with the exception of the asphalt waterstops, which used a linear model. Val-

ues for the fitting parameter m and residual wetting phase saturation S_{lr} , and equations for the threshold pressure P_t for the materials in the lower shaft model may be found in Statham et al. (1997).

The centerline of the shaft is assumed to be a no-flow boundary. The outer radial boundary at 282 m is assumed to be a constant-pressure boundary at hydrostatic equilibrium relative to 12.5 MPa in Marker Bed 139 near the base of the repository. The top and bottom of the cylindrical grid are assumed to be no-flow boundaries, since the initial pressure gradients are primarily directed radially inward due to the atmospheric pressure condition of the open shaft during the repository operational period. The exception is the gas flow from the repository. This is simulated by applying a time-varying pressure and constant gas-saturation boundary condition at the base of the shaft.

5 ANALYSES AND RESULTS

To examine the effects of crushed salt consolidation on performance, two types of simulations were performed: 1.) Permeability model. The crushed-salt consolidation was modeled as a change in permeability of the crushed-salt column as a function of pore pressure and depth. The porosity of the crushed salt was a constant, 0.05. This was Statham's base case, and will be used here for comparison purposes. 2.) Log-linear model. The porosity function of pore pressure and depth was used for the crushed-salt column. Two different log-linear fits of permeability versus porosity were used to couple porosity and permeability.

5.1 Permeability model

The permeability model handles the consolidation of crushed salt by changing the permeability of the crushed salt. Figure 4 shows the permeability of crushed salt as a function of fractional density. Data from the structural analysis calculations was used in conjunction with this permeability data to define a time rate of change in permeability as a function of pressure and depth. Salt column permeability varies from $2.5 \times 10^{-15} \text{ m}^2$ at the initial fractional density of 0.9 to $6.3 \times 10^{-21} \text{ m}^2$ at the maximum fractional density of 1.0. Details can be found in Statham et al. [1997]. This was a simulation Statham performed, and we will use it here as a base case for comparison purposes. Porosity of the crushed salt was held constant at 0.05. The repository gas pressure boundary condition increased from 1.75 MPa at the beginning of the simulation to 7 MPa by 100 years.

Figure 5 shows the gas saturations for the base case. The radial extent for this figure has been trun-

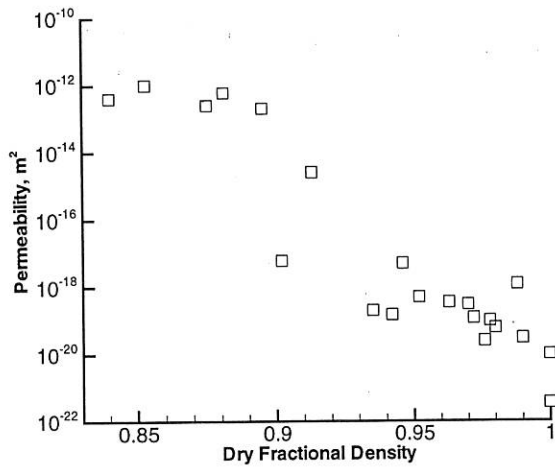


Figure 4. Permeability versus dry fractional density.

cated at 4 m to show details in the shaft. The higher gas saturation right above the lower concrete plug at 565-590 m is associated with low pressure. Statham referred to this as a gas 'bubble'. Gas saturations in this gas 'bubble' are as high as 0.65. Gas saturations in this gas 'bubble' are as high as 0.65. Gas saturation is also apparent below and above marker bed 138 (MB138, depth ~640 m) with saturations to 0.5; in the DRZ at the depth of the lower asphalt waterstop (~610 m) with saturations of 0.5 to 0.6; and at the top of the crushed salt column (~430 m) with gas saturations of 0.08. These gas bubbles only extend as far as the edge of the shaft or the associated DRZ. The rest of the shaft and formation have become nearly brine-saturated.

The solid line in figure 6 represents the absolute permeability in the shaft versus depth for this simulation. The salient feature here is the low permeability seen from 565-585 m, in the salt column. The low permeability coincides with the gas bubble in the salt column, where the lowered pressure allows

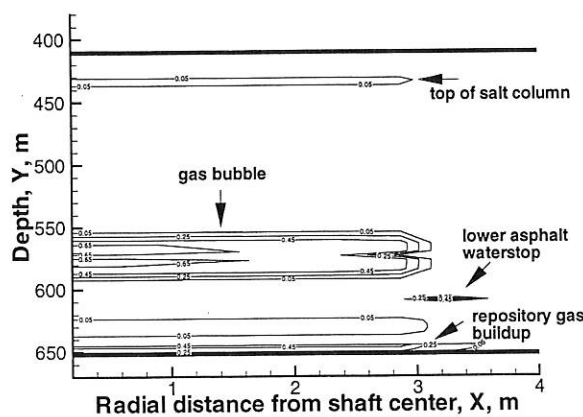


Figure 5. Gas saturation contours for the permeability model, 100 years.

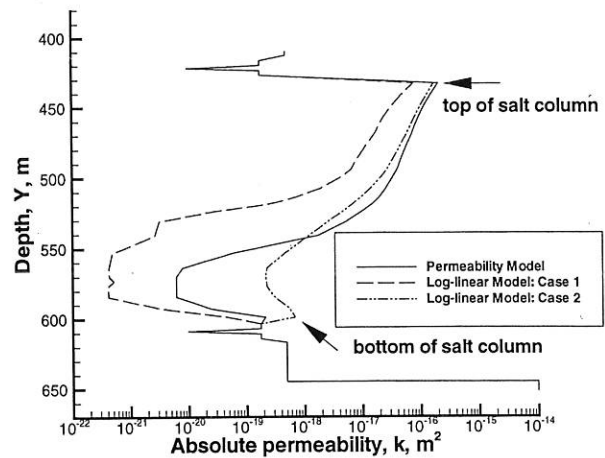


Figure 6. Absolute permeability in the shaft, 100 years.

more salt consolidation, and hence, a lower permeability. From 565 to 585 m, permeability is about $6 \times 10^{-21} \text{ m}^2$. Below 585 m and above 565 m, permeability increases with depth.

In summary, gas from the repository is blocked from vertical movement by the presence of MB138 (at a depth of 645 m). The gas saturations seen below MB138 and in the DRZ at the lower concrete plug are associated with the repository gas input. Since MB138 saturates with brine early in the simulation due to its higher permeability compared to the formation (MB138 has a permeability of $1 \times 10^{-19} \text{ m}^2$ and is fully brine-saturated by 25 years), and hence shows higher pressure, MB138 blocks the transmission of gas (with its lower pressure) from the repository into the shaft. The permeability of the lower Salado clay ($5 \times 10^{-19} \text{ m}^2$ from 617-645 m) is lower than that of the shaft station monolith below it ($1 \times 10^{-14} \text{ m}^2$) which probably blocks some of the transport from the shaft station monolith to the lower Salado clay, and thus allows the pressure build up below 640 m. Gas from the lower Salado clay is also blocked from vertical transmission. The lower asphalt waterstop has a permeability of $1 \times 10^{-20} \text{ m}^2$. This low permeability does not allow much upward vertical movement of gas from the lower Salado clay. Also, there is higher pressure along MB134 (at 600 m) consistent with its lower permeability and subsequent brine saturation. This high pressure also serves to block transport of the gas in the lower Salado clay component of the seal.

The gas bubble in the salt column is caused by a combination of higher pressure occurring in the upper part of the crushed salt column due to brine saturation from the marker beds, and by the lowering of permeability in the crushed salt due to the consolidation. The marker beds in the upper part of the crushed salt column have permeabilities that are

several orders of magnitude higher than the marker beds near the lower portion of the salt column. Therefore, brine flow along *MB123* and Union Anhydrite causes the upper part of the salt column to saturate with brine. Because of this, gas in the lower portion of the salt column becomes trapped by the higher pressures above. At the same time, the lower pressures in the gas bubble cause more consolidation to occur at that depth range, thus causing lower permeability in that region, trapping the gas from further transport. The gas saturation in the *DRZ* at 431 m is a remainder of the gas initially in the asphalt waterstop.

Finally, the permeability in the salt column changes. Generally, we'd expect the permeability to increase with increasing depth, with the bottom of the column showing lower permeabilities (more consolidation) than the top of the column. However, since permeability also depends on the pressure in the shaft, we see the permeability in the gas bubble showing the lowest values. The permeability at the location of the gas bubble is the lowest, at $6 \times 10^{-21} \text{ m}^2$. The permeability at the top of the salt column is about $1 \times 10^{-16} \text{ m}^2$.

5.2 Log-linear models

In the log-linear models, the porosity of the crushed salt varied as a function of pore pressure and depth. The crushed salt porosity and permeability were coupled. Figure 4 shows the permeability of crushed salt as a function of fractional density. The first fit, Case 1, set the permeability of the crushed salt as $1.0 \times 10^{-14} \text{ m}^2$ at a porosity of 0.1 and $1.0 \times 10^{-24} \text{ m}^2$ at a porosity of 0.01 (Knowles, pers. comm.) The equation coupling porosity and permeability was:

$$k = 7.75 \times 10^{-26} e^{255.8\phi} \quad (10)$$

where k = permeability in m^2

A second permeability/porosity coupling, Case 2, was used to examine the sensitivity of the performance to the permeability/porosity functions. For Case 2, a linear fit was made to the data on a semi-log plot. This fit gave a permeability of $2.5 \times 10^{-15} \text{ m}^2$ at a porosity of 0.1 and a permeability of $6.3 \times 10^{-21} \text{ m}^2$ at a porosity of 0.01. The equation coupling porosity and permeability was:

$$k = 1.51 \times 10^{-21} e^{143.3\phi} \quad (11)$$

The models coupling porosity and permeability was implemented in *TOUGH28W* and 100-year simulations were performed.

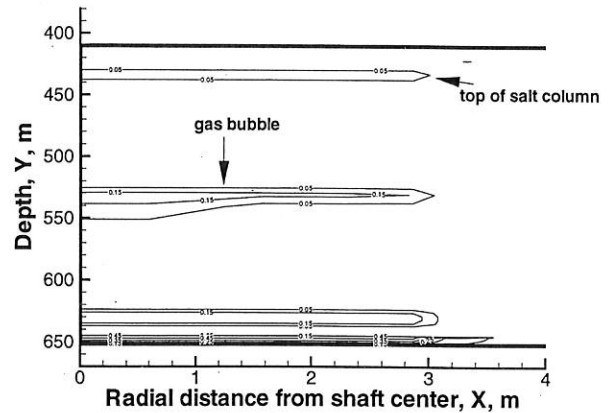


Figure 7. Gas saturation contours for the log-linear model, 100 years.

Case 1. Figure 7 shows the gas saturation contours; the radial direction has been truncated to 4 m to show details in the shaft. There is a region of higher gas saturation in the salt column at 525-550 m, with a maximum saturation of 0.17, and a radial extent to 3 m. From 428-438 m there is another region with gas saturation, with maximum saturation of 0.08, and a radial extent to 3 m. Both of these areas of gas saturation are consistent with the pressure contours seen in the model output. Elsewhere the crushed-salt column has become saturated with brine. Below 625 m, the gas saturations shown are similar to those described for the permeability case.

The solid line in figure 8 represents the porosity in the shaft. The lowest porosity in the salt column occurs from 550 to 585 m, with a value of 0.035. Below 585 m, the porosity increases to a value of 0.05 at the bottom of the salt column. From 550 to 530 m, the porosity increases slowly to 0.04. Above 530 m, porosity increases more rapidly to a value of 0.07 at 490 m. From 490 m to the top of the salt column, porosity increases slowly, to a value of 0.08.

The dashed line in figure 6 represents the permeability in the shaft. The lowest permeability in the salt column occurs from 555 to 585 m, with a value of $4 \times 10^{-22} \text{ m}^2$. Below 585 m, permeability steadily increases to a value of $2 \times 10^{-19} \text{ m}^2$ at a depth of 603 m. Above 555 m, permeability increases, reaching a value of $3 \times 10^{-21} \text{ m}^2$ at 540 m. Above this, permeability increases further, reaching a value of $7.4 \times 10^{-17} \text{ m}^2$ at 433 m. There is a fast increase in permeability from 500 to 530 m, and a slower increase from 433 to 500 m.

In summary, there is an area of gas saturation in the salt column from 525 to 540 m. By 50 years, the pressure in the shaft at 480-515 m is already much higher than the surrounding pressures. The magnitude is nearly 2.5 MPa. There is also high pressure at

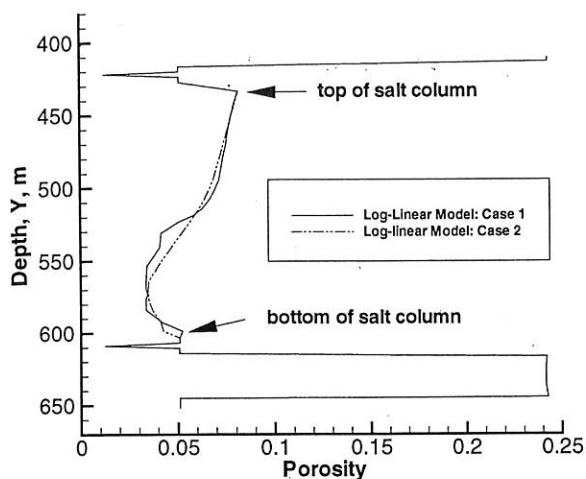


Figure 8. Porosity in the shaft, 100 years.

590 to 605 m, with magnitudes around 7 MPa. No other simulation shows this early pressure increase in the shaft. The permeability is the key to understanding the pressure behavior. The high pressure seen below 590 m occurs because the permeability at 590 m is so tight due to salt column consolidation. This causes the pressure below to build up, because fluid cannot dissipate upwards. A similar situation occurs below 490 m. Higher pressure occurs there compared to the other cases due to the presence of MB123. Pressure builds up because of the high permeability of MB123 that forms a conduit to the undisturbed boundary. The upper portion of the salt column has high permeability. This allows the column to become brine saturated with brine from MB123. High pressures then occur in the upper salt column because of the brine saturation. The lower part of the salt column has lower permeability (compared to the upper part of the salt column) and doesn't allow much transport, either brine transport from the radial boundary and formation, or gas transport from the salt column to other parts of the shaft or formation. Therefore the region of gas saturation in the salt column is formed by a combination of the higher pressures caused by brine inflow along marker beds, and by the lowered permeability in the salt column due to consolidation. This is similar to the situation that occurred in the permeability model; however, the higher initial porosity and permeability in the salt column for the log-linear model allows more brine inflow, and thus we have much higher pressures in the salt column compared to the permeability model. The pressure also increases in the salt column due to the porosity decrease due to consolidation.

Case 2. The overall trend is similar to Case 1. Gas saturation of similar magnitude to Case 1 is seen in the salt column at a slightly different depth (545-

560 m), and the corresponding pressures are higher (at around 7-8 MPa). The pressures in the lower part of the salt column are lower (around 9 MPa), and similar pressures are seen in the upper salt column. The dash-dot-dot line in figure 8 shows the porosity in the shaft. The minimum porosity seen is 0.035 from 565-580 m. The porosity at the top of the salt column is 0.08, and is 0.04 at the bottom of the salt column. The porosity for Case 2 is very similar to that of Case 1. The dash-dot-dot line in figure 6 shows the permeability in the shaft. The minimum permeability in the salt column is $2 \times 10^{-19} \text{ m}^2$ from 560-580 m, the permeability at the top of the salt column is $2 \times 10^{-16} \text{ m}^2$, and the permeability at the bottom of the salt column is $7 \times 10^{-19} \text{ m}^2$. The permeability for the Case 2 model is higher, compared to Case 1.

6 DISCUSSION

TOUGH28W was modified to handle variable porosity with pore pressure and depth. This involved code changes so that the fluid mass balance was not adversely affected. One of the objectives of the salt column modeling analyses was to determine the permeability and porosity of the crushed salt column with time. For the simulations performed with variable crushed salt porosity, none achieved a porosity consistent with intact salt (0.01). The lowest porosities seen in the 100-year simulation period were in the range of 0.027 to 0.035. Generally, the lowest porosities occurred in the lower portion of the crushed salt column. For the simulations with variable permeability, the lowest permeabilities in the salt column for a 100-year simulation range from $4 \times 10^{-22} \text{ m}^2$ for the log-linear model, Case 1, to $2 \times 10^{-19} \text{ m}^2$ for the log-linear model, Case 1. The permeabilities were generally lower in the lower portion of the crushed salt column.

From the results, it is apparent that the permeability function chosen affects the consolidation of the salt column greatly. For the permeability model, the minimum permeability in the crushed salt column achieves a value consistent with fully-healed salt. The minimum permeability occurs in the region of higher gas saturation in the salt column. For simulations where the permeability and porosity are allowed to vary, the permeability does not achieve values consistent with intact salt. Although a region of gas saturation is seen in the salt column for the coupled porosity/permeability simulations, this region is much smaller, has lower gas saturations, and has higher pressure compared to the permeability model. Part of the salt column pressurization is due to the change in volume because of the porosity decrease with consolidation. It is also likely that the

higher initial porosity (0.1) allowed more fluid transport into the shaft, compared to the permeability model, with its constant crushed salt porosity of 0.05.

Future work includes comparing results between the lower shaft model (used here) and a full shaft model. If there are substantial differences in the predictions between the two models, these simulations should be performed on a full shaft model. Calculations could be done to examine the effects of different repository boundary conditions, as was done by Statham using the permeability model. It would also be interesting to examine the effects of the two-phase models and parameters, especially as the selection of two-phase models and parameters could have a strong effect on the gas trapped in the salt column. Work is planned on coupling *TOUGH28W* to a rock mechanics code, which will simulate the salt consolidation in a more thorough manner. In order to simulate the volume changes due to salt consolidation, plans are underway to implement a moving grid capability in *TOUGH28W*.

REFERENCES

- Brodsky, N.S. 1994. Hydrostatic and Shear Consolidation Tests with Permeability Measurements on Waste Isolation Pilot Plant Crushed Salt. *SAND93-7058*. Albuquerque, New Mexico: Sandia National Laboratories.
- Brooks, R.H. & Corey, A.T. 1996. Properties of Porous Media Affecting Fluid Flow. In *Proceedings of the American Society of Civil Engineers (ASCE), Journal of Irrigation and Drainage Division* 33(IR2): 61-88.
- Callahan, G.D. 1999a. Crushed Salt Constitutive Model. *SAND98-2680*. Albuquerque, New Mexico: Sandia National Laboratories.
- Callahan G.D. 1999b. Final Monthly Progress Report for Sandia Contract AG-4911 Covering the Time Period February 1, 1999, Through March 14, 1999. Albuquerque, New Mexico: Sandia National Laboratories.
- Christian-Frear, T. 1996. User's Manual for *TOUGH28W*, Version 2.00. *WPO #36535*. Albuquerque, New Mexico: Sandia National Laboratories.
- Davies, P.B. 1991. Evaluation of the Role of Threshold Pressure in Controlling Flow of Waste-Generated Gas into Bedded Salt at the Waste Isolation Pilot Plant. *SAND90-3246*. Albuquerque, New Mexico: Sandia National Laboratories.
- Holcomb, D.J. & Zeuch, D.H. 1990. Modeling the consolidation of a porous aggregate of dry salt as isostatic hot pressing. *Journal of Geophysical Research* 95(310): 15611-15622.
- Javeri, V. 1998. Combined Gas and Nuclide Transport in a two dimensional Repository considering a variable Rock Convergence. In *Proceedings of the TOUGH Workshop '98, LBNL-41995, CONF-980559: 77-82*. Berkeley, California: Lawrence Berkeley Laboratories.
- Parker, J.C., Lenhard, R.L., & Kuppusamy, T. 1987. A Parametric Model for Constitutive Properties Regarding Multiphase Flow in Porous Media. *Water Resource Research* 23(4): 618-624.
- Pruess, K. 1987. *TOUGH User's Guide*, Nuclear Regulatory Commission Report. *LBL-20700*. Berkeley, California: Lawrence Berkeley Laboratories.
- Pruess, K. 1991. *TOUGH2—A General-Purpose Numerical Simulator for Multiphase Fluid and Heat Flow*. *LBL-29400*. Berkeley, California: Lawrence Berkeley Laboratories.
- Sandia. 1996. Waste Isolation Pilot Plant Shaft Sealing System Compliance Submittal Design Report, Volumes 1 and 2. *SAND96-1326/1&2*. Albuquerque, New Mexico: Sandia National Laboratories.
- Statham, William H., Kelley, V., & Knowles, M.K. 1997. Fluid Flow Analysis of the Lower Salado Components of the Waste Isolation Pilot Plant Shaft Sealing System Design. Austin, Texas: Duke Engineering and Services, Inc.
- van Genuchten, M. 1980. A Closed-Form Equation for Predicting the Hydraulic Conductivity of Unsaturated Soils. *Soil Science Society of America Journal* 44(5):892-898.
- Webb, S.W. 1996. Review of Two-Phase Characteristic Curves for Porous Media and Application to the WIPP. *SAND93-3912*. Albuquerque, New Mexico: Sandia National Laboratories.
- Zeuch, D.H. 1990. Isostatic hot-pressing mechanism maps for pure and natural sodium chloride—Applications to nuclear waste isolation in bedded and domal salt formations. *International Journal of Rock Mechanics and Mining Sciences & Geomechanics Abstracts* 27(6):505-524.